A note on the time-frequency analysis of GW150914

Patrick Flandrin

A note on the time-frequency analysis of GW150914

Patrick Flandrin
Univ Lyon, Ens de Lyon, Univ Claude Bernard,
CNRS, Laboratoire de Physique, F-69342 Lyon, France
flandrin@ens-lyon.fr

September 22, 2016

Abstract

This note summarizes in a sketchy way some findings (filtering, parameter estimation, comparison with models) that have been obtained with time-frequency analyses of the gravitational wave signals corresponding to the event GW150914, as detected by LIGO on Sept. 14, 2016.

1 Data

The first direct observation of a gravitational wave emitted by the merger of a binary black hole has recently been reported [1], soon after followed by a second announcement [2].

We will here focus on the first observation, which consists in two transient signals of short-duration (a fraction of a second) associated to an event referred to as GW150914, as detected on Sept. 14, 2015 by the two LIGO giant interferometers located respectively in Hanford, WA and Livingston, LA.

The corresponding data has been made publicly available at the LIGO website (see `https://losc.ligo.org/events/GW150914/`), together with additional information such as numerical relativity models for the observed waveforms.

2 Time-frequency analysis

The event GW150914 corresponds to the merger of two black holes, entering the category of transient bursts that are characterized by a "chirp" signature, with an increase in both amplitude and instantaneous frequency during the inspiral part that precedes the coalescence. As it has already been observed many times (see, e.g., [6, 7] or [11]), this peculiar structure suggests to perform the analysis in a time-frequency domain, giving the signature the simple form of a trajectory in the plane.

2.1 Spectrogram and reassigned spectrogram

As far as time-frequency analysis is concerned, many possibilities are offered [4, 8], and we will here make only use of simple and well-established techniques based on the short-time Fourier transform (STFT), namely the spectrogram (squared magnitude of the STFT) and its reassigned version (whose purpose is to dramatically increase the localization of chirps in the plane [12, 3, 9].

Thanks to these techniques, the chirping nature of the two recorded waveforms is clearly evidenced, see Figure 1.

In both cases, the observation is made of 3441 data points, sampled at the rate of $16,384$ Hz. The TF analysis (spectrogram and its reassigned version) has been made with a time step of 8 samples and a frequency zoom in on the lower part of the spectrum by a factor of 24. This results in a TF matrix of size 431×85, covering the effective TF domain [0.25 s, 0.46 s] $\times$ [0 Hz, 341 Hz]. The short-time window is a Gaussian whose size (1,023 samples) has been chosen to be almost "circular" (see [10]) for the retained sampling of the TF plane. All calculations have been made in Matlab, using scripts of the Time-Frequency ToolBox that is available at `http://tftb.nongnu/org`.

2.2 Filtering from spectrogram zeros

A new technique [10] has recently been proposed for disentangling multicomponent nonstationary signals into coherent AM-FM structures, thus making possible a time-frequency filtering of chirp-like signals. In contrast with conventional techniques (e.g., ridges [5]) that tend to identify components with "large" values of the transform, the new approach is only based on the zeros (that are known to completely characterize the transform (and, hence, the signal) for the proper choice of a "circular" Gaussian window [13]).

Considering zeros as nodes for a Delaunay triangulation [14], the key observation [10] is that, in noise only situations, triangles have edges that obey a given, regular, distribution whereas, when a signal component is added, its presence is marked by longer edges. In a nutshell, the method proceeds therefore as follows:

1. Perform a Delaunay triangulation over the spectrogram zeros;
2. Identify outlier edges (with respect to the edge length distribution in the noise-only case);
3. Keep triangles with at least one outlier edge;
4. Group adjacent such triangles in connected, disjoint domains;
5. Multiply the STFT with labeled 1/0 masks attached to the different components;
6. Reconstruct the disentangled components, domain by domain, by using standard reconstruction formulæ.

As for the reconstruction step, it can be achieved by using either the standard 2D formula or its simplified, yet exact 1D form:

$$x_j(t) = \frac{1}{g(0)} \int_{(t,\omega)\in\mathcal{D}_j} F_x^{(g)}(t,\omega)\, \frac{d\omega}{2\pi} \tag{1}$$

where $F_x^{(g)}(t,\omega)$ stands for the STFT with window g of the signal x, and $\mathcal{D}_j$ for the j-th selected TF domain.

2.3 GW150914 analyses

In order to fix the threshold for discriminating outlier edges, the edge distribution is estimated from a number of surrogate spectrograms computed on noise only signals, under the same conditions as the ones used for the signal under test. A further specification can be added with respect to area: in case a Delaunay cell would have a "too small" area while having at least one outlier edge (in terms of length), the cell is rejected. This is illustrated in Figure 2 in the case of the Hanford signal, with the result of the overall proposed procedure of TF filtering in Figure 3.

The case of the Livingston signal proved to be more noisy, and thus more difficult to handle in an automatic way. One possibility would be to supervise the analysis and complete by hand the selection of relevant triangles. Because the proposed approach to TF filtering is fundamentally based on zeros, another option is however possible, which consists in adding a small amount of noise to the observation prior its analysis. This results in a slight perturbation of the zeros constellation that may lead to more favourable triangulations (this noise-aided technique has to be explored further). The Livingston counterpart of the previous Hanford analyis is reported in Figures 4 and 5.

3 Comparisons

3.1 Filtered data vs. models

Besides observed data, results of numerical gravity computations are also available, and thus amenable to comparisons between theory and measurements. Such a comparison is reported in Figure 6, evidencing in both cases an amazing agreement.

3.2 Hanford vs. Livingston

Since both Hanford and Livingston signals are supposed to correspond to the same event, it is possible to make them coincide after a proper shift related to the propagation, at the speed of light, of the gravitational wave from one detector to the next.

The geometry of the system indicates that such a shift should involve a phase term of π radians as well as a time delay of at most 10 ms, given that

the two detectors are distant from about $3,000$ km. This expectation is clearly supported by Figure 7 in which is plotted the cross-correlation between the two filtered waveforms. The shape of this cross-correlation function is nearly symmetric, with a negative peak off the origin. The fact that this peak is negative evidences the phase shift of π radians that is expected in between the waveforms, due to the relative positioning of the detectors. Furthermore, the time distance at which the peak is located from the origin turns out to be of 6.8 ms, corresponding to an effective, acceptable distance of $2,000$ km. (Let us remark that the detection in Hanford following that in Livingston, this suggests that the event took place in the Southern Hemisphere.)

Figure 8 displays the similarity between the two filtered waveforms, once properly synchronized according to the above mentioned shifts as well as to an *ad hoc* amplitude adjustement.

3.3 Chirp parameters estimation

Once the observations have been filtered, one can go further and estimate the chirp parameters under the assumption that the inspiral part of the coalescence (before it attains its maximum and then evolves in a different ring-down mode) follows the approximation that describes the way the amplitude and the instantaneous frequency diverge when approaching the coalescence time t_0. Indeed, according to a first post-Newtonian approximation, the waveform expected to be observed from a coalescing binary reads (see, e.g., [15] or [16]):

$$x(t; t_0, C) = A(t_0 - t)^{-\alpha} \cos\left(2\pi d(t_0 - t)^{\beta} + \varphi\right) \Theta(t_0 - t),$$

where A stands for the amplitude, $\alpha = 1/4$, $\beta = 5/8$, φ is a phase factor, $\Theta(.)$ the unit step function, and d the "chirp rate". This last coefficient quantifies the power-law divergence of the instantaneous frequency which reads [6]:

$$f_x(t) = \frac{5d}{8}(t_0 - t)^{-3/8}\Theta(t_0 - t).$$

This chirp rate d happens to be related to the so-called "chirp mass" $\mathcal{M}$, a quantity that combines the masses of the two coalescing objects, according to the relation $d = 160 \times 3^{3/8}\mathcal{M}_{\odot}^{-5/8}$ (where $\mathcal{M}_{\odot} = \mathcal{M}/M_{\odot}$ and $M_{\odot}$ stands for the solar mass) [15, 6], thus allowing to convert estimated chirp rates into chirp masses.

Given this model, two main parameters have therefore to be estimated, namely the coalescence time t_0 and the chirp mass $\mathcal{M}_{\odot}$. The classical approach for such a task is to make use of a bank of matched filters [15] but, as suggested in [6, 7], an (approximate) equivalent formulation can be given in the time-frequency plane: it suffices to perform a path integration along trajectories that precisely correspond to the instantaneous frequency model. Examples of this strategy are reported in Figures 9 and 10 (Hanford signal), and Figures 11 and 12 (Livingston signal). One can observe coherent results, though with an increased contrast when using a reassigned spectrogram in place of a conventional one. The obtained values for the chirp mass range from 27.8 to 28.9 solar

masses, with an average value of 28.5 solar masses which is pretty consistent with what is reported in [1].

References

[1] B.P. Abbott *et al.*, "Observation of gravitational waves from a binary black hole merger," *Phys. Rev. Lett.*, Vol. 116, pp. 061102-1-061102-16, 2016.

[2] B.P. Abbott *et al.*, "GW151226: Observation of gravitational waves from a 22-solar-mass binary black hole coalescence," *Phys. Rev. Lett.*, Vol. 116, pp. 241103-1-241103-14, 2016.

[3] F. Auger and P. Flandrin, "Improving the readability of time-frequency and time-scale representations by the reassignment method," *IEEE Trans. on Acoust., Speech and Signal Proc.*, Vol. 43, No. 5, pp. 1068–1089, 1995.

[4] B. Boashash (ed.), *Time-Frequency Signal Analysis and Processing - A Comprehensive Reference*, 2nd Edition, Academic Press, 2016.

[5] R. Carmona, W. Hwang, and B. Torresani, "Characterization of signals by the ridges of their wavelet transforms," *IEEE Trans. on Signal Proc.*, Vol. 45, pp. 2586?-2590, 1997.

[6] E. Chassande-Mottin, P. Flandrin, "On the time-frequency detection of chirps," *Appl. Comp. Harm. Anal.*, Vol. 6, No. 2, pp. 252-281, 1999.

[7] E. Chassande-Mottin, P. Flandrin, "On the time-frequency detection of chirps and its application to gravitational waves," in *Second Workshop on Gravitational Wave Data Analysis*, pp. 47-52, Éditions Frontires, 1999.

[8] P. Flandrin, *Time-Frequency/Time-Scale Analysis*, Academic Press,1999.

[9] P. Flandrin, F. Auger, and E. Chassande-Mottin, "Time-frequency reassignment — From principles to algorithms," in *Applications in Time-Frequency Signal Processing*, A. Papandreou-Suppappola, Ed., chapter 5, pp. 179–203, CRC Press, Boca Raton (FL), 2003.

[10] P. Flandrin, "Time-frequency filtering from spectrogram zeros," *IEEE Signal Proc. Lett.*, Vol. 2, No. 11, pp. 2137-2141, 2015.

[11] J.-M. Innocent and B. Torrésani, "Wavelets and binary coalescences detection," *Appl. Comp. Harm. Anal.*, Vol. 4, No. 1, pp. 113–116, 1997.

[12] K. Kodera, R. Gendrin and C. de Villedary, "Analysis of time-varying signals with small BT values, *IEEE Trans. on Acoust., Speech and Signal Proc.*, Vol. ASSP-26, No. 1, pp.64–76,1978.

[13] H.J. Korsch, C. Muller, and H. Wiescher, "On the zeros of the Husimi distribution," *J. Phys. A: Math. Gen.*, Vol. 30, pp. L677–L684, 1997.

[14] A. Okabe, B. Boots, K. Sugihara, and S.N. Chiu, *Spatial Tessellations — Concepts and Applications of Voronoi Diagrams* (2nd ed.), John Wiley, 2000.

[15] B. S. Sathyaprakash and S. V. Dhurandhar, "Choice of filters for the detection of gravitational waves from coalescing binaries," *Phys. Rev. D*, Vol. 44, pp. 3819?-3834, 1991.

[16] K. S. Thorne, "Gravitational radiation," in *300 Years of Gravitation* (S. W. Hawking and W. Israel, dds.), pp. 330–458, Cambridge Univ. Press, Cambridge, 1987.

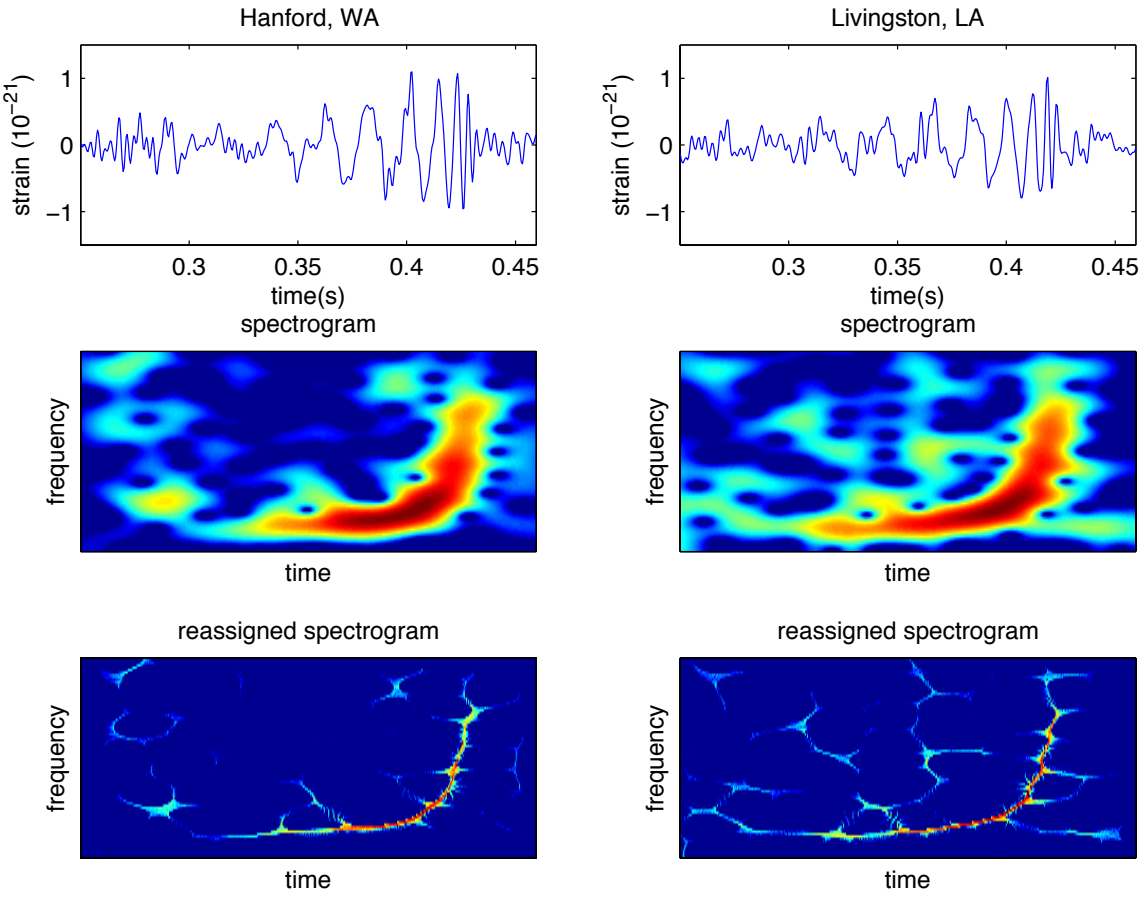

Figure 1: **Waveforms and time-frequency signatures** — *Left column: Hanford, WA; Right column: Livingston, LA. In both cases, the waveforms (top row) have a "chirping" time-frequency signature, as evidenced by a spectrogram (middle row) and its reassigned version (bottom row). The displayed frequency range of the analysis is [0 Hz, 341 Hz].*

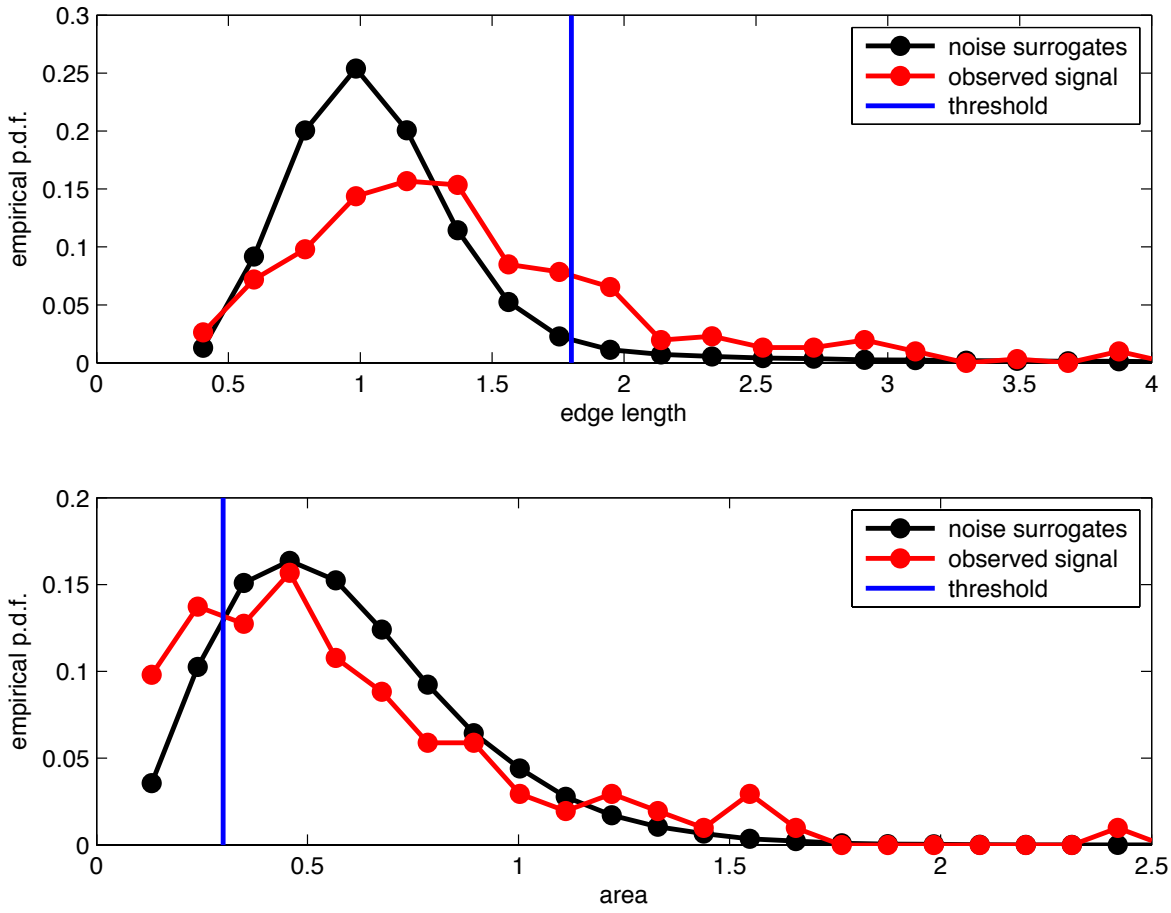

Figure 2: **Delaunay triangles selection (Hanford)** — *Comparing the distribution of geometrical attributes of the Delaunay triangles (top: edge length, bottom: cell area) of the observed data (red) with those of a set of* 500 *noise surrogates (black) used as null reference, permits to fix thresholds (blue) for retaining outlier triangles with a given false alarm rate.*

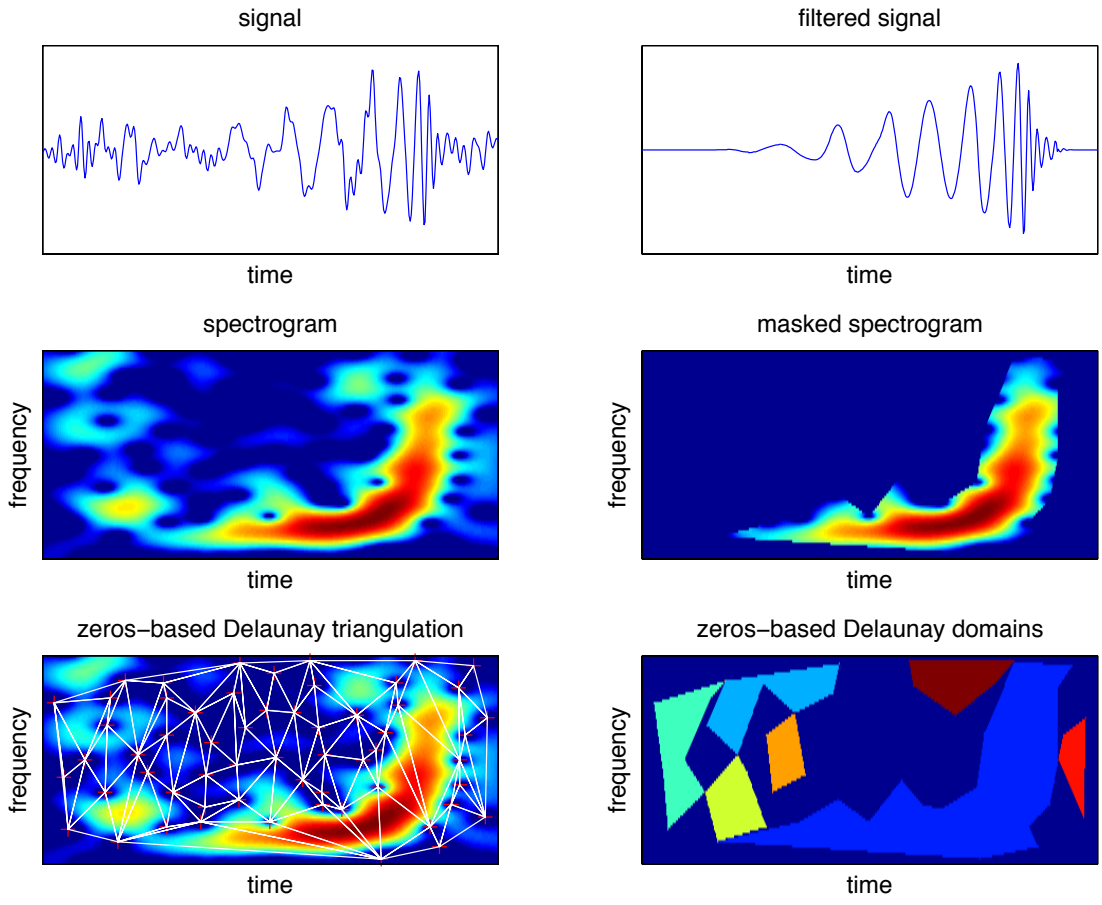

Figure 3: **Time-frequency filtering (Hanford)** — *Top left: original signal (noisy observation). Middle left: spectrogram. Bottom left: spectrogram with the Delaunay triangulation based on its zeros. Bottom right: Delaunay domains obtained by concatenating adjacent triangles with at least one outlier edge and sufficient area. Middle right: TF filtered spectrogram, as masked by the indicator function of the (blue) Delaunay domain of interest. Top right: filtered signal obtained from the masked short-time Fourier transform.*

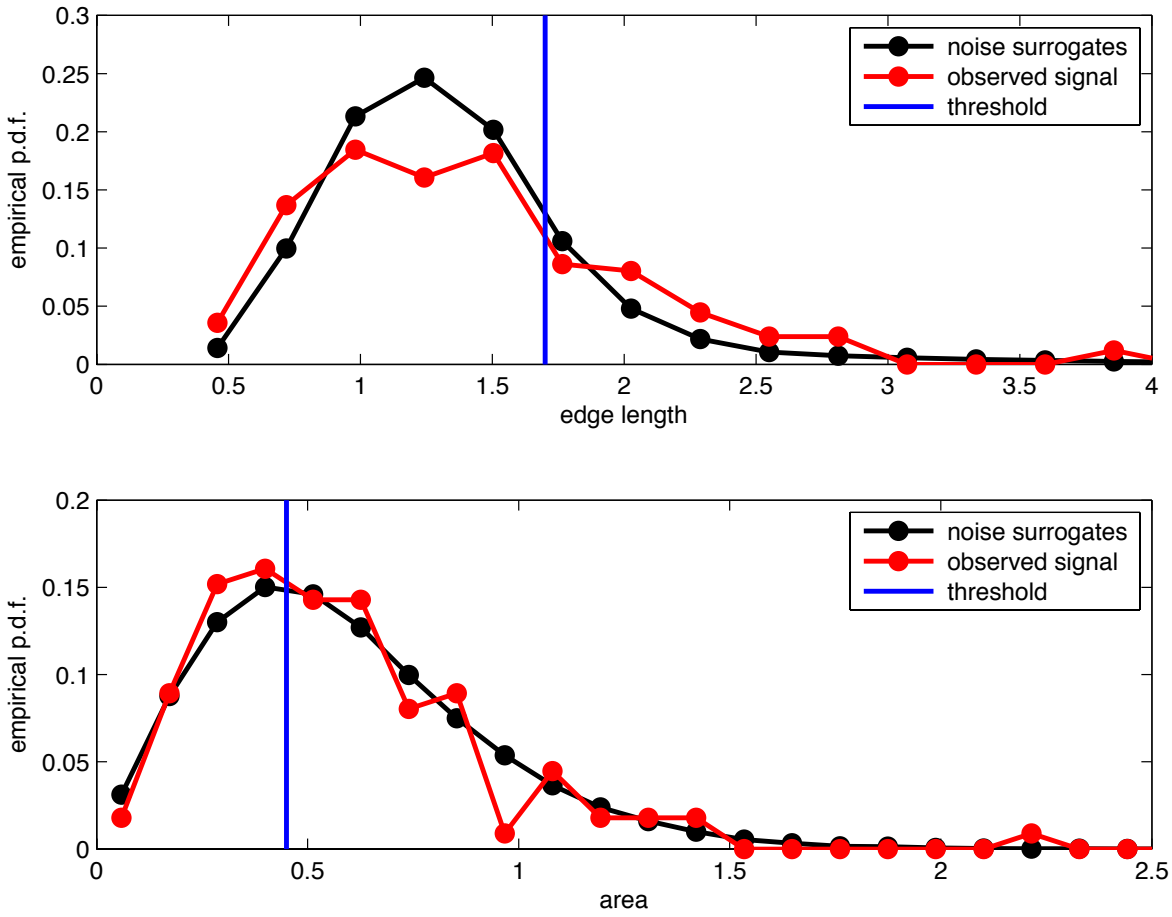

Figure 4: **Delaunay triangles selection (Livingston)** — *Comparing the distribution of geometrical attributes of the Delaunay triangles (top: edge length, bottom: cell area) of the observed data (red) with those of a set of* 500 *noise surrogates (black) used as null reference, permits to fix thresholds (blue) for retaining outlier triangles with a given false alarm rate.*

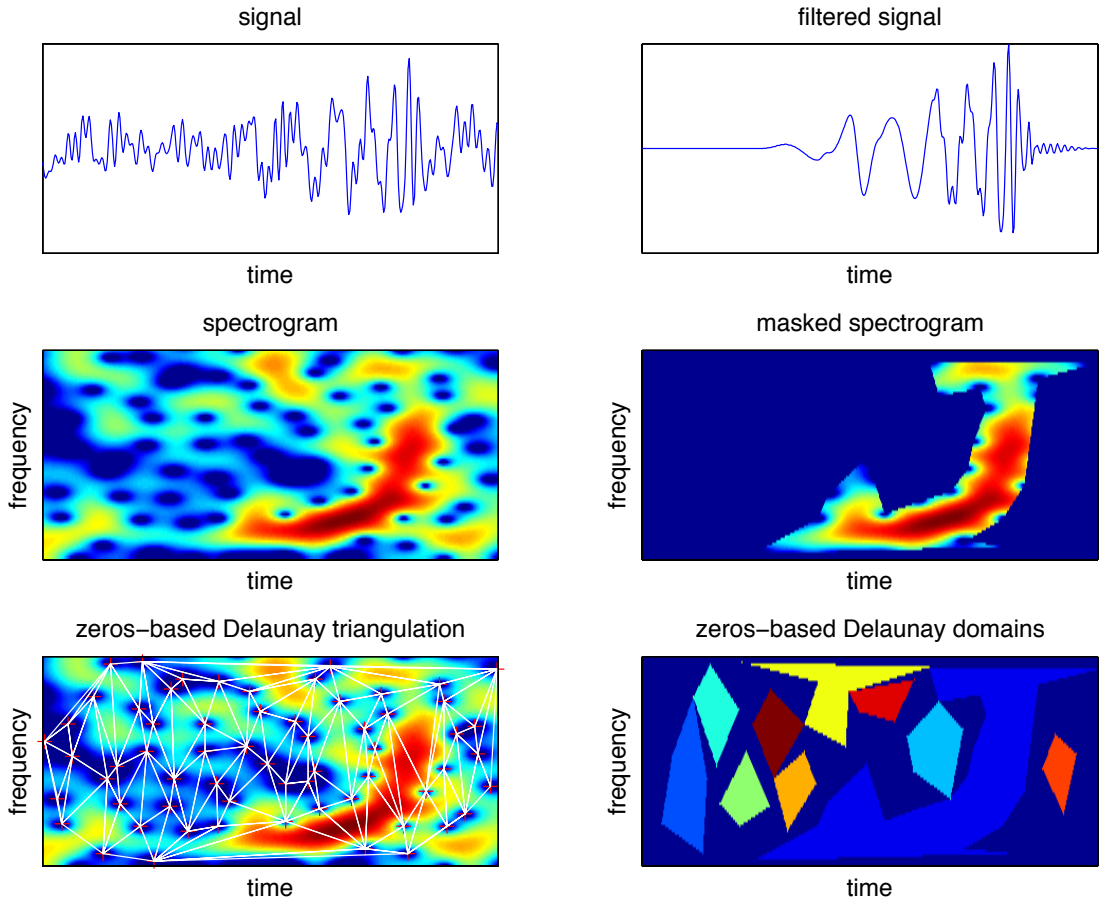

Figure 5: **Time-frequency filtering (Livingston)** — *Top left: original signal (noisy observation). Middle left: spectrogram. Bottom left: spectrogram with the Delaunay triangulation based on its zeros. Bottom right: Delaunay domains obtained by concatenating adjacent triangles with at least one outlier edge and sufficient area. Middle right: TF filtered spectrogram, as masked by the indicator function of the (blue) Delaunay domain of interest. Top right: filtered signal obtained from the masked short-time Fourier transform.*

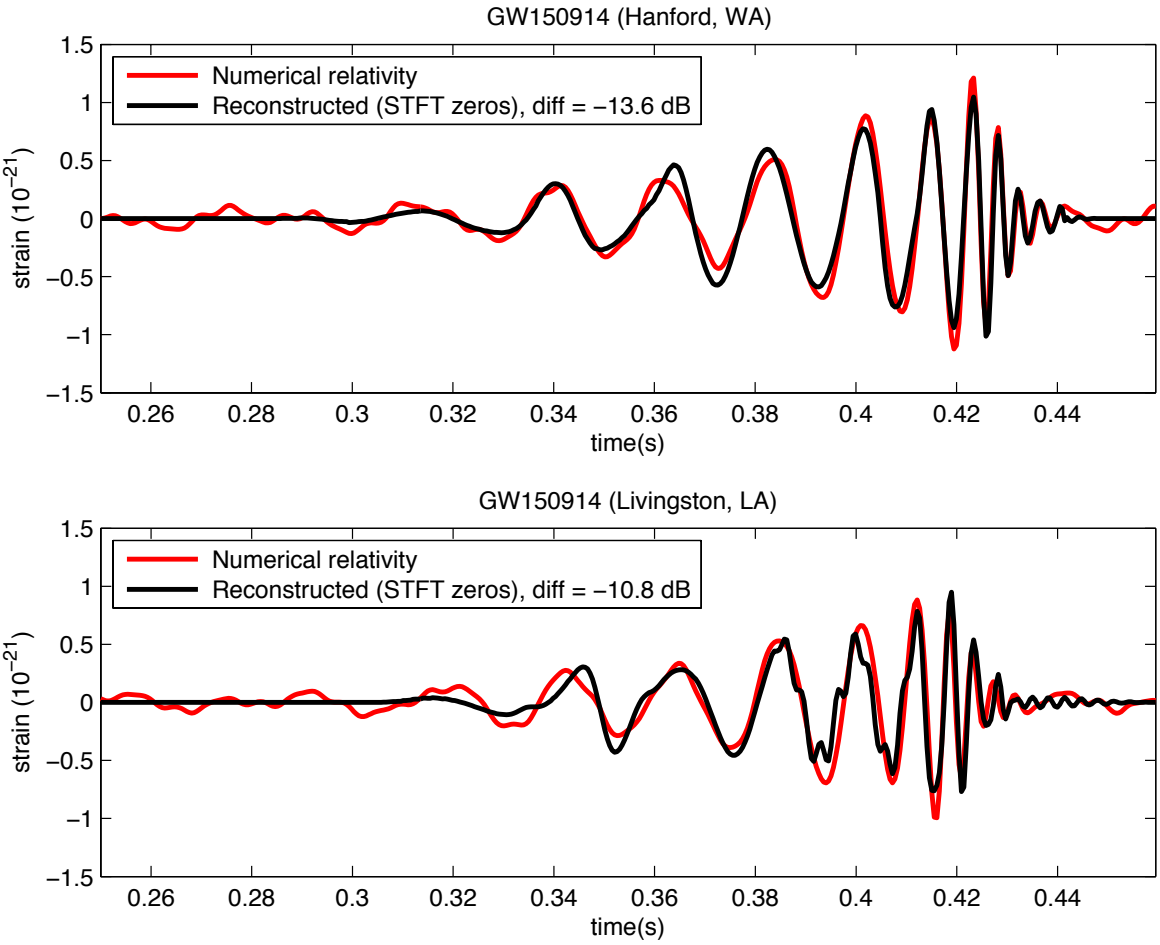

Figure 6: **Reconstruction and model** — *Superimposition of the filtered signal (black) and of the model computed by numerical relativity (red), evidencing an amazing agreement in both cases of the Hanford signal (top) and Livingston signal (bottom).*

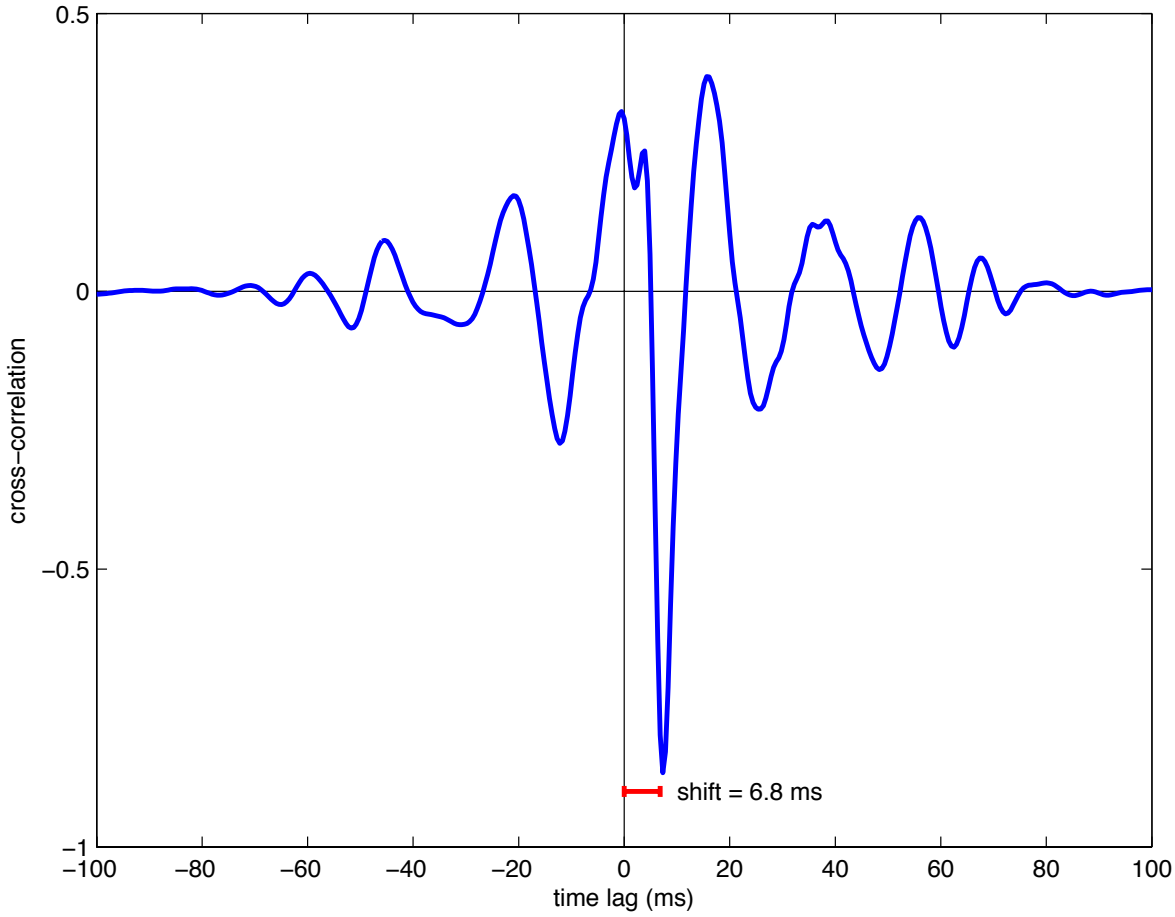

Figure 7: **Cross-correlating Hanford and Livingston signals** — *The cross-correlation between the (TF filtered) Hanford and Livingston signals is nearly symmetric, with a negative peak off the origin. This supports the expected claim that, due to propagation and the relative positioning of the detectors, the two observations differ by a phase shift of* π *radians and a time shift of* 6.8 *ms.*

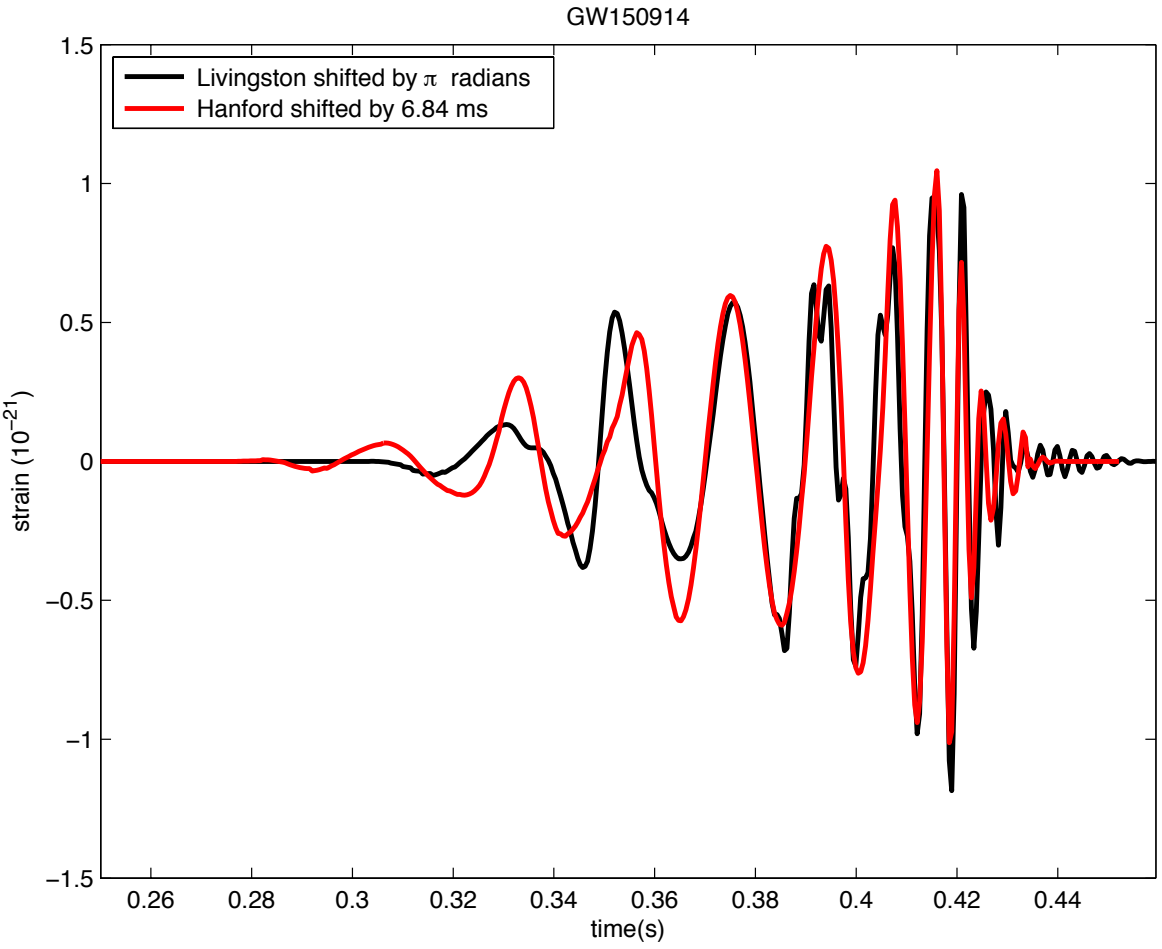

Figure 8: **Hanford and shifted Livingston** — *Superimposition of the filtered Hanford signal (red), shifted in time by* 6.84 *ms, and of the filtered Livingston signal (black), shifted in phase by* π *radians.*

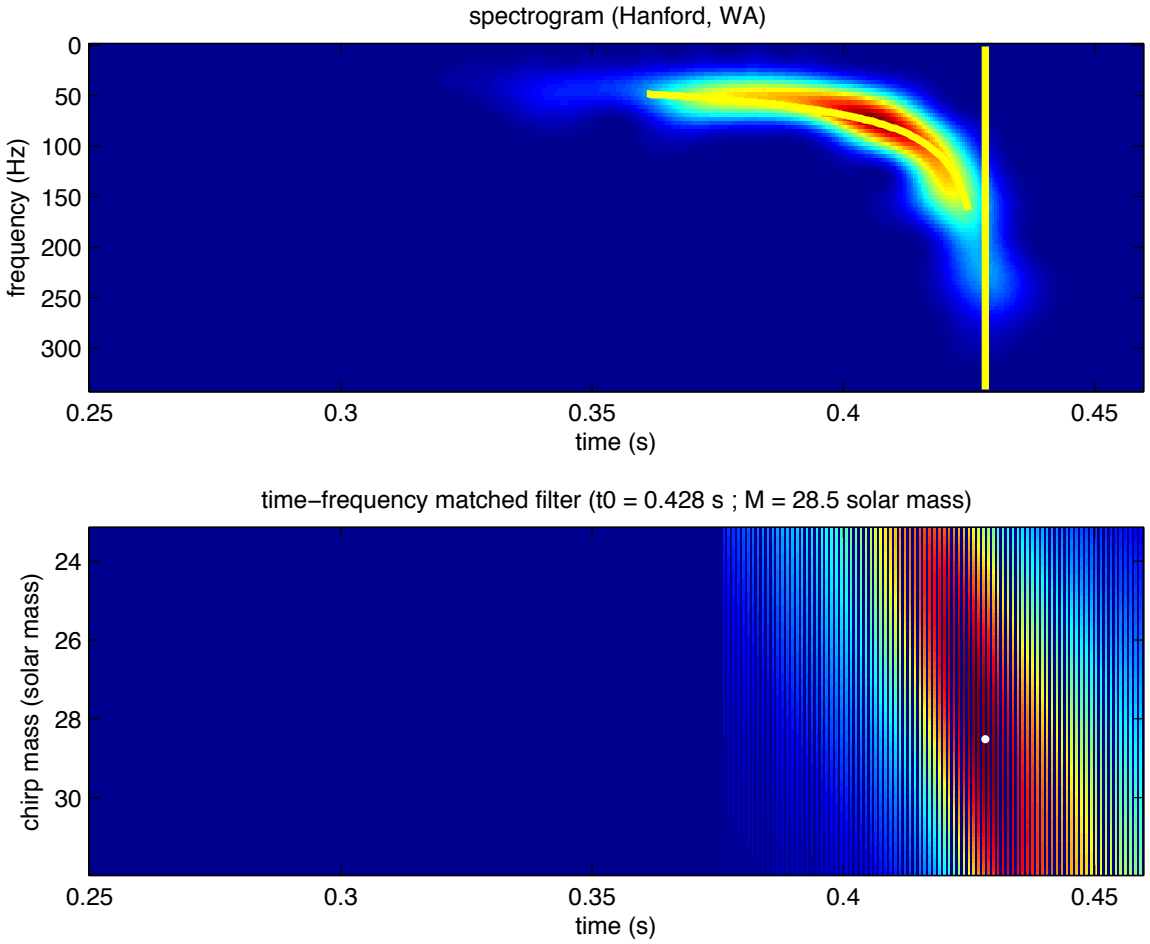

Figure 9: **Parameters estimation from spectrogram (Hanford)** — *Bottom: output of the time-frequency matched filter obtained by the path integration of a spectrogram along the instantaneous frequency curve of the binary coalescence model, as a function of the chirp mass and of the coalescence time (maximum is indicated by the white dot). Top: spectrogram of the filtered signal, with the optimum model trajectory and the corresponding coalescence time superimposed in yellow.*

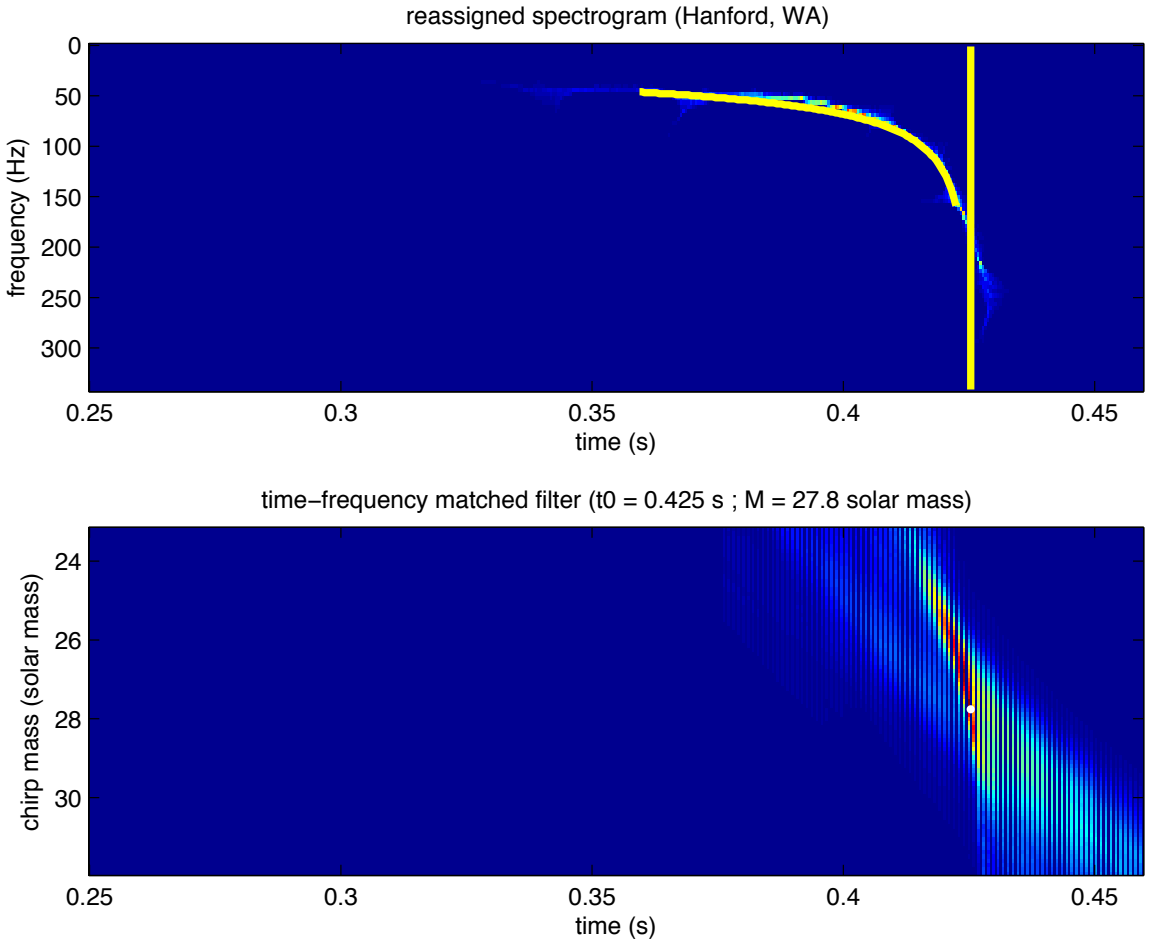

Figure 10: **Parameters estimation from reassigned spectrogram (Hanford)** — *Bottom: output of the time-frequency matched filter obtained by the path integration of a reassigned spectrogram along the instantaneous frequency curve of the binary coalescence model, as a function of the chirp mass and of the coalescence time (maximum is indicated by the white dot). Top: reassigned spectrogram of the filtered signal, with the optimum model trajectory and the corresponding coalescence time superimposed in yellow.*

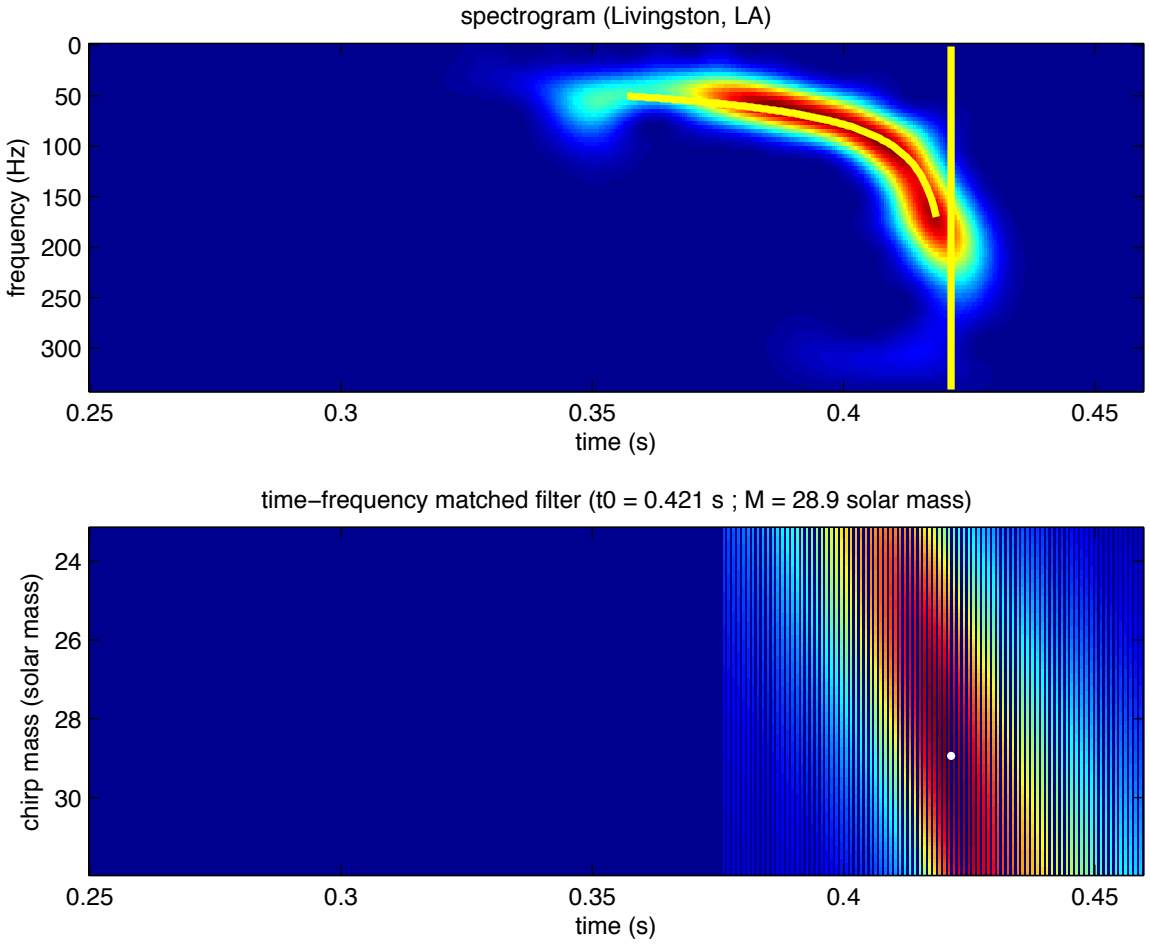

Figure 11: **Parameters estimation from spectrogram (Livingston)** — *Bottom: output of the time-frequency matched filter obtained by the path integration of a spectrogram along the instantaneous frequency curve of the binary coalescence model, as a function of the chirp mass and of the coalescence time (maximum is indicated by the white dot). Top: spectrogram of the filtered signal, with the optimum model trajectory and the corresponding coalescence time superimposed in yellow.*

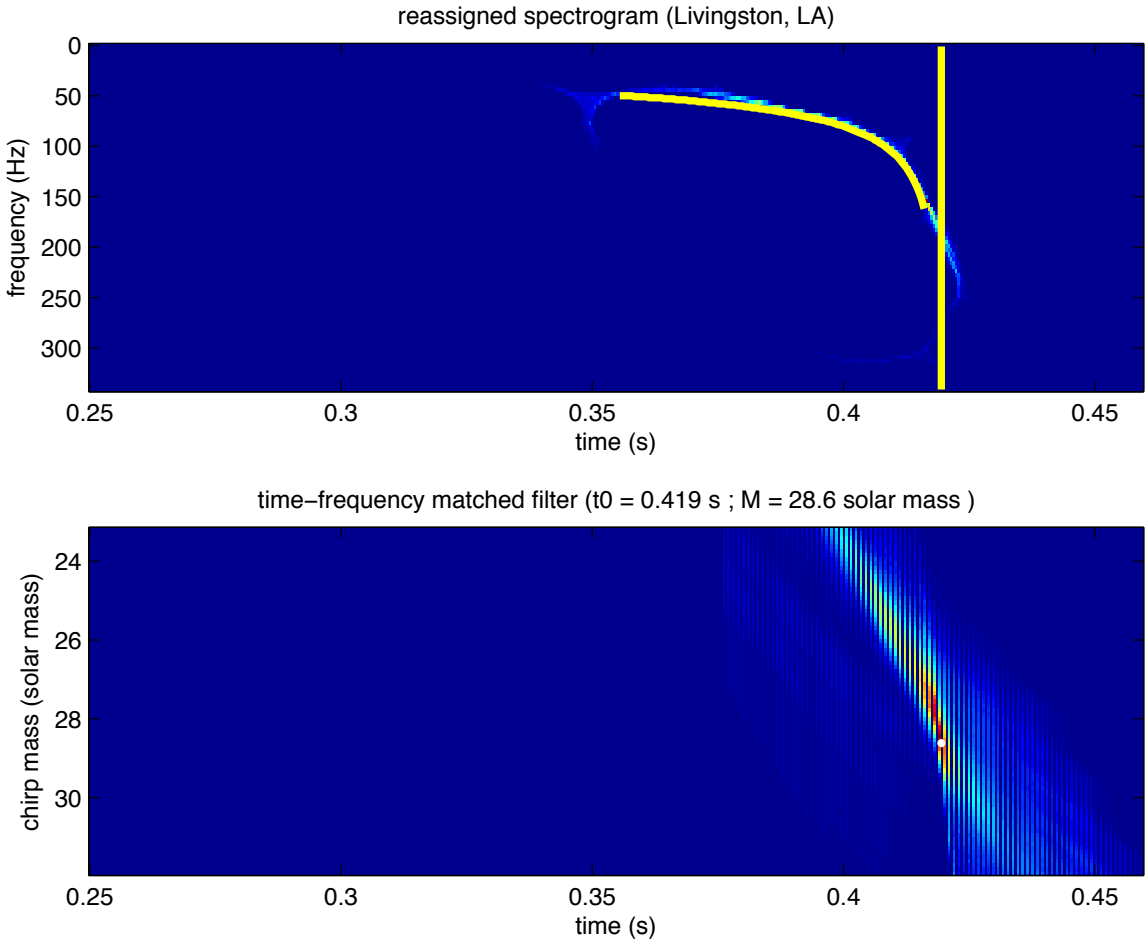

Figure 12: **Parameters estimation from reassigned spectrogram (Livingston)** — *Bottom: output of the time-frequency matched filter obtained by the path integration of a reassigned spectrogram along the instantaneous frequency curve of the binary coalescence model, as a function of the chirp mass and of the coalescence time (maximum is indicated by the white dot). Top: reassigned spectrogram of the filtered signal, with the optimum model trajectory and the corresponding coalescence time superimposed in yellow.*